

Movable Antenna-Aided Secure LEO Satellite Networks: Joint Antenna Position and Beamforming Optimization

Suhong LUO¹, Pan TANG^{1*}, Jianhua ZHANG¹, Ji WANG², Yixuan LI²,
Zihang DING¹ & Xingwang LI³

¹State Key Laboratory of Network and Switching Technology, Beijing University of Posts and Telecommunications,
Beijing 100876, China

²College of Physical Science and Technology, Central China Normal University, Wuhan 430079, China

³School of Physics and Electronic Information, Henan Polytechnic University, Jiaozuo 454003, China

Abstract The broadcast characteristics of sixth-generation (6G) low-earth orbit (LEO) satellite communications raise serious security issues. Movable antenna (MA) technology offers a promising physical layer security (PLS) solution by flexibly reconfiguring antenna positions to exploit additional spatial degrees of freedom. However, in highly dense LEO satellite constellations, the legitimate satellite and potential eavesdropping satellites may exhibit small angular separations, which poses significant challenges for the design of secure transmission schemes. To address this challenge, this paper proposes an MA-assisted secure transmission scheme for time-varying LEO satellite communications, where a ground station equipped with an MA array communicates with a serving satellite, while the other visible satellites are regarded as potential eavesdroppers. We maximize the average secrecy rate by jointly optimizing the transmit beamforming and MA positions. An alternating optimization (AO) framework is developed, where semidefinite relaxation is adopted for the beamforming optimization subproblem, while high-accuracy successive convex approximation (SCA) and low-complexity differential evolution (DE) algorithms are proposed for the MA position optimization subproblem. Numerical results demonstrate that the proposed MA-assisted LEO secure transmission scheme consistently achieves superior performance compared to the conventional fixed-position antenna scheme.

Keywords 6G, LEO satellite networks, movable antenna, physical layer security, transmit beamforming, antenna position optimization.

Citation

. Sci China Inf Sci, for review

1 Introduction

Driven by the demand for global seamless coverage and ubiquitous connectivity in sixth-generation (6G) networks, satellite communications have become a key component of non-terrestrial networks (NTNs). In particular, low-earth orbit (LEO) satellite networks are regarded as promising enablers of space-air-ground integrated networks (SAGINs), owing to their wide coverage, flexible deployment, and relatively low transmission latency [1–3]. However, the open and broadcast characteristics of satellite channels makes them vulnerable to eavesdropping, posing serious security risks [4–6]. Such risks are further exacerbated in LEO constellations due to rapid satellite motion and high satellite density.

Physical layer security (PLS) has been widely regarded as a promising complement to conventional cryptographic techniques for secure wireless transmission. By exploiting the inherent differences between legitimate and eavesdropping channels, PLS can prevent confidential information leakage from an information-theoretic perspective [7]. In satellite communication systems, PLS-based secure transmission schemes have been extensively studied [8–15]. Nevertheless, most existing studies rely on fixed-position antenna (FPA) frameworks, whose array geometry is pre-determined after deployment. Consequently, their steering vectors are fixed, limiting their ability to adapt the spatial channel responses, suppress eavesdropping channels, and enhance secure transmission.

Fluid antenna systems (FASs) and movable antenna (MA) provide a solution to overcome the aforementioned limitations. Unlike conventional FPA systems with fixed array geometries, FAS/MA allows antenna elements to adjust their positions within predefined regions, thereby introducing additional spatial degrees-of-freedom (DoFs) for array manifold reconfiguration beyond conventional beamforming [16]. In highly dynamic large-scale LEO satellite

* Corresponding author (email: tangpan27@bupt.edu.cn)

constellations, the legitimate satellite and potential eavesdropping satellites may exhibit small angular separations. MA arrays can enlarge the effective array aperture through antenna position reconfiguration, thereby improving angular resolution and enhancing the discrimination between legitimate and eavesdropping channels [17].

Existing studies have investigated the fundamental principles, implementation architectures, and key challenges of FAS/MA technologies. They show that by exploiting the spatial response of wireless channels, FAS/MA technologies can reshape the array manifold, improve channel conditions, and enhance spatial resolution [18–20]. For FASs, the authors of [21] proposed a fluid-antenna-enabled secret communications, where port selection was exploited to improve secrecy performance. The authors of [22] further investigated coding-enhanced cooperative jamming for FAS-assisted secret communication, where port selection and power control were jointly designed to maximize the secrecy rate. Existing studies have established a field-response channel model for MA systems and analyzed the impact of antenna position variations on channel gain and communication performance [23,24]. The authors of [25] studied secure wireless communication via an MA array and demonstrated that antenna position optimization can effectively enhance secrecy performance against multiple eavesdroppers. The authors of [26] investigated secure MIMO communication with MAs, showing that antenna movement at both the transmitter and receiver yields significant secrecy gains over conventional FPA systems. The authors of [27] extended MA-assisted PLS to full-duplex multi-user communications, where artificial noise, beamforming, and antenna positions are jointly optimized. The authors of [28] further considered robust secure design under scenarios where instantaneous channel state information (CSI) of eavesdroppers is unavailable, showing that MA can still achieve stable secrecy rates through geometric reconfiguration. Beyond explicit secure transmission, the authors of [29] introduced MA into covert communications, illustrating that positional DoFs can also serve to conceal the existence of transmission.

However, research on MAs in satellite communications is still relatively limited. Existing representative works focus mainly on a few directions. [17] studied MA-enabled dynamic beam coverage in satellite communications. By jointly optimizing the antenna position and beamforming, the scheme minimizes average leakage power under coverage gain constraints, addressing the time-varying coverage and interference in LEO constellations. Results show that MA achieves better adaptability to time-varying coverage requirements compared to conventional fixed arrays. [30] further considered the application of MA in full-duplex satellite communications, studying power-efficient transmission design and demonstrating that MA can enhance both spectral and power efficiency in full-duplex satellite links through geometric reconfiguration. Furthermore, [31] introduced the MA array into the design of LEO ground station (GS), studying the joint optimization of array element positions and time-varying beamforming weights, verifying the capability of MA arrays to suppress interference and enhance transmission rates in LEO networks. Although these works have demonstrated the feasibility and value of integrating MA with satellite communications, the inherent broadcast nature and highly dynamic topology of LEO networks make secure transmission a critical issue.

To the best of our knowledge, this paper is the first work to investigate MA-enabled secrecy rate optimization in LEO satellite uplink communications. In particular, we consider a dynamic LEO satellite constellation, where a GS equipped with an MA-based uniform planar array (UPA) transmits confidential information to its serving satellite, while all other satellites are treated as potential eavesdroppers. The main contributions are summarized as follows

- Based on the considered system, we formulate an average secrecy rate maximization problem by jointly optimizing the MA positions and the GS transmit beamforming. The optimization is subject to the secrecy rate constraints, the transmit power constraints, and the movement region constraints of all antenna elements. To reduce the movement overhead, the MA positions are determined during the initialization phase and kept fixed throughout the entire communication period of the GS.
- To solve this non-convex problem, we develop a high-accuracy successive convex approximation (SCA)-based alternating optimization (AO) algorithm. Specifically, the coupling between the antenna position vector and the transmit beamforming vector is handled within an AO framework. Next, semidefinite relaxation (SDR) combined with Gaussian randomization is employed to optimize the time-varying beamforming vector, while the antenna position vector is updated via the SCA method.
- To reduce the complexity of MA position optimization, we also propose a low-complexity differential evolution (DE) algorithm. Specifically, the beamforming subproblem is also solved via SDR. Then, a high-quality MA position is acquired by using a DE-based algorithm. A DE-based population search approach is adopted to optimize the MA positions without requiring gradient information, yielding an efficient low-complexity solution.
- Numerical results demonstrate that 1) the proposed MA-assisted LEO satellite communications significantly outperforms the conventional FPA scheme in terms of secrecy performance; 2) as the number of satellites increases, the MA elements tend to move outward to enlarge the array aperture, thereby improving the angular resolution for distinguishing the legitimate satellite from potential eavesdroppers and enhancing the secrecy performance; and 3) the relative performance of the SCA-based and DE-based AO algorithms depends on the antenna number.

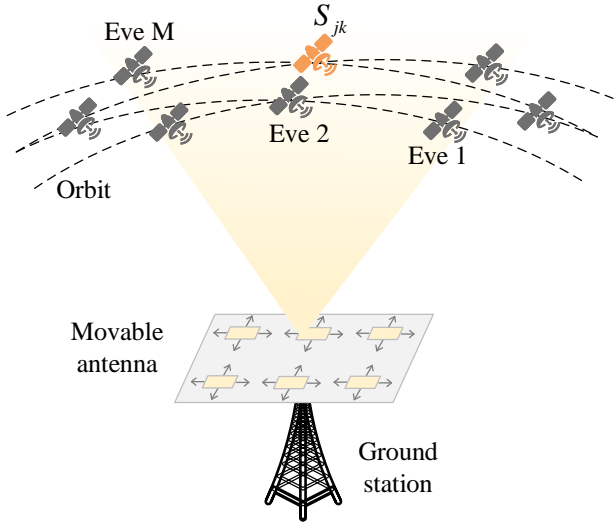


Figure 1 Illustration of an MA-aided uplink secure LEO constellation.

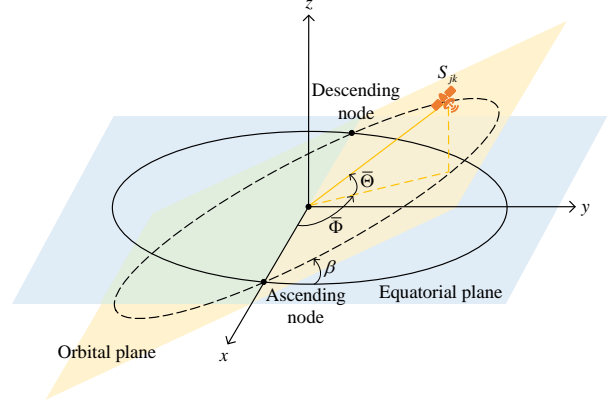


Figure 2 Geometric illustration of a LEO satellite orbit [17].

Specifically, DE achieves better performance with a small number of antennas due to its global search capability, whereas when the number of antennas becomes large, the expanded search space weakens the effectiveness of DE, allowing SCA to achieve superior performance.

2 SYSTEM MODEL AND PROBLEM FORMULATION

2.1 System Model

As shown in Fig. 1, we consider an uplink communication scenario where a GS equipped with an MA array communicates with a set of LEO satellites arranged in a Walker Delta constellation [31]. The GS transmits the uplink signal to the serving LEO satellite, while the remaining visible satellites on the same orbital shell act as passive eavesdroppers attempting to eavesdrop the signal. A Walker Delta constellation with J orbital planes is considered, where each orbital plane contains K uniformly distributed satellites. For simplicity, we focus on the orbital segment from the South Pole to the North Pole for each orbital plane. The k -th LEO satellite in the j -th orbital plane is denoted as S_{jk} , where $j \in \mathcal{J} \triangleq \{1, 2, \dots, J\}$, $k \in \mathcal{K} \triangleq \{1, 2, \dots, K\}$. Fig. 2 shows the spatial geometry of a LEO satellite orbit in the geocentric spherical coordinate system (GSCS).

All the LEO satellites are assumed to move in circular orbits at a common altitude H above the Earth's surface. The position of S_{jk} at the continuous time instant t in the GSCS is described by

$$\bar{R} = R + H, \quad (1)$$

$$\bar{\Theta}_{jk}(t) = \arcsin[\sin \beta \sin \alpha_{jk}(t)], \quad (2)$$

$$\bar{\Phi}_{jk}(t) = \arctan[\cos \beta \tan \alpha_{jk}(t)] + \frac{2\pi j}{J}, \quad (3)$$

where R denotes the Earth's radius, $\bar{\Theta}_{jk}(t) \in [-\pi/2, \pi/2]$ and $\bar{\Phi}_{jk}(t) \in (-\pi, \pi]$ denote the geocentric latitude and the geocentric longitude of satellite S_{jk} , respectively. β denotes the orbital inclination. The geocentric angle of S_{jk} with respect to the ascending node at time t is expressed as $\alpha_{jk}(t) = 2\pi t/T + \alpha_{jk0}$, where $\alpha_{jk0} = -\pi/2 + \pi(k-1)/(K-1)$ denotes the initial angle at $t = 0$. The J orbital planes are uniformly spaced in azimuth, and the ascending node of the j -th plane is offset by $2\pi j/J$ from the reference meridian on the equatorial plane. The orbital period is given by $T = 2\pi\sqrt{\bar{R}^3/G_e M_e}$, where G_e and M_e represent the gravitational constant and the Earth's mass, respectively.

Accordingly, the LEO satellite coordinates in the 3D geocentric Cartesian coordinate system (GCCS) can be expressed as

$$\mathbf{R}_{jk}(t) = [\bar{R} \cos \bar{\Theta}_{jk}(t) \cos \bar{\Phi}_{jk}(t), \bar{R} \cos \bar{\Theta}_{jk}(t) \sin \bar{\Phi}_{jk}(t), \bar{R} \sin \bar{\Theta}_{jk}(t)]^T. \quad (4)$$

The GS is located at a fixed point on the Earth's surface. In the adopted GCCS, its coordinates vary with time due to the Earth's rotation. Thus, the position of GS is denoted as

$$\mathbf{R}_G(t) = [R \cos \Theta_G \cos \Phi_G(t), R \cos \Theta_G \sin \Phi_G(t), R \sin \Theta_G]^T, \quad (5)$$

where Θ_G denotes the geocentric latitude of the GS, and $\Phi_G(t) = 2\pi t/T_E$ represents the time-varying geocentric longitude, with T_E being the Earth's rotation period.

2.2 Channel Model

To characterize the array response of the MA array, we further introduce a GS centric Cartesian coordinate system (SCCS) with its origin located at the GS. In the SCCS, the y -axis points toward the local east direction, the z -axis is oriented radially outward from the Earth's center, and the x -axis lies in the local tangent plane toward the local north direction, thereby forming a right-handed coordinate system. Let \mathbf{T} denotes the transformation matrix from the SCCS to the GCCS. According to the above definition of the axis, \mathbf{T} can be written as

$$\mathbf{T}(t) = \begin{bmatrix} -\sin \Theta_G \cos \Phi_G(t) & -\sin \Phi_G(t) \cos \Theta_G \cos \Phi_G(t) \\ -\sin \Theta_G \sin \Phi_G(t) & \cos \Phi_G(t) \cos \Theta_G \sin \Phi_G(t) \\ \cos \Theta_G & 0 & \sin \Theta_G \end{bmatrix}. \quad (6)$$

For the uplink transmission, the propagation direction from the GS to satellite S_{jk} in the GCCS is described by

$$\mathbf{d}_{jk}(t) = \mathbf{R}_{jk}(t) - \mathbf{R}_G(t). \quad (7)$$

The corresponding wave vector in the GCCS is expressed as

$$\mathbf{b}_{jk}(t) = \frac{2\pi \mathbf{d}_{jk}(t)}{\lambda \|\mathbf{d}_{jk}(t)\|_2}, \quad (8)$$

where λ denotes the wavelength at the carrier frequency. By applying the coordinate transformation, the wave vector in the SCCS is given by

$$\tilde{\mathbf{b}}_{jk}(t) = \mathbf{T}(t)^T \mathbf{b}_{jk}(t). \quad (9)$$

Let the position of the n -th MA element in the SCCS be denoted as $\bar{\mathbf{c}}_n$

$$\bar{\mathbf{c}}_n = [x_n, y_n, z_n]^T, \quad (10)$$

where $n \in \mathcal{N} \triangleq \{1, \dots, N\}$. Without loss of generality [31], we assume that each MA element can only move within the local horizontal plane. Hence, we always have $z_n = 0$, and the antenna position can be equivalently expressed as

$$\bar{\mathbf{c}}_n = [\mathbf{c}_n^T, 0]^T, \quad \mathbf{c}_n \in \mathcal{C} \subset \mathbb{R}^2, \quad (11)$$

where \mathcal{C} denotes the 2D movable area of the antenna elements. Collectively, the MA position vector is defined as

$$\mathbf{c} = [\mathbf{c}_1^T, \mathbf{c}_2^T, \dots, \mathbf{c}_N^T]^T, \quad (12)$$

which determines the geometry of the MA array. Hence, the transmit steering vector of the MA array towards satellite S_{jk} at time t is given as

$$\mathbf{s}_{jk}(\tilde{\mathbf{b}}_{jk}(t), \mathbf{c}) = [e^{j\tilde{\mathbf{b}}_{jk}(t)^T \bar{\mathbf{c}}_1}, \dots, e^{j\tilde{\mathbf{b}}_{jk}(t)^T \bar{\mathbf{c}}_N}]^T. \quad (13)$$

For the channel from the GS to satellite S_{jk} , the corresponding large-scale channel gain is modeled as

$$\rho_{jk}(t) = \rho_0 \|\mathbf{d}_{jk}(t)\|_2^{-\alpha}, \quad (14)$$

where ρ_0 is the path gain at a reference distance $d_0 = 1$ m, α is path loss exponent. It is assumed that every antenna unit employs an isotropic radiation pattern in the half-space directed downward. The uplink channel model between the MA array and satellite S_{jk} given by

$$\mathbf{h}_{jk}(\mathbf{c}, t) = \sqrt{\rho_{jk}(t)} e^{j\frac{2\pi}{\lambda} \|\mathbf{d}_{jk}(t)\|_2} \mathbf{s}_{jk}(\tilde{\mathbf{b}}_{jk}(t), \mathbf{c}), \quad (15)$$

Among all visible satellites, we select one satellite $S_{j_0 k_0}$ as the legitimate receiver. For notational simplicity, we refer to this satellite as S_L . The channel and received signal at S_L can be written as

$$\mathbf{h}_L(\mathbf{c}, t) = \mathbf{h}_{j_0 k_0}(\mathbf{c}, t), \quad (16)$$

$$y_L(\mathbf{c}, \mathbf{w}(t), t) = \mathbf{w}(t)^H \mathbf{h}_L(\mathbf{c}, t) x(t) + n_L(t), \quad (17)$$

where $\mathbf{w}(t)$ denotes the GS transmit beamforming vector, and $x(t)$ denotes the transmit signal from the GS. $n_L(t)$ is additive noise at S_L . The remaining visible satellites on the same orbital shell act as passive eavesdroppers. Let $\mathcal{M} \triangleq \{1, \dots, M\}$ denotes the index set of such eavesdropping satellites. Denote the m -th eavesdropping satellite by $S_{E,m} = S_{j_m k_m}$, $m \in \mathcal{M}$. Collectively, we denote eavesdropping satellite set as $\Omega \triangleq \{S_{E,1}, \dots, S_{E,M}\}$. Specifically, the eavesdropping channel is modeled as

$$\mathbf{h}_{E,m}(\mathbf{c}, t) \triangleq \mathbf{h}_{j_m k_m}(\mathbf{c}, t). \quad (18)$$

The receive signal of eavesdropping satellite $S_{E,m}$ can be written as¹⁾

$$y_{E,m}(\mathbf{c}, \mathbf{w}(t), t) = \mathbf{w}(t)^H \mathbf{h}_{E,m}(\mathbf{c}, t) x(t) + n_{E,m}(t), \quad (19)$$

where $n_{E,m}(t)$ denotes the received noise at the m -th eavesdropping satellite. The received signal-to-noise ratios (SNRs) at the legitimate satellite S_L and the m -th eavesdropping satellite $S_{E,m}$ are given as

$$\gamma_L(\mathbf{c}, \mathbf{w}(t), t) = \frac{|\mathbf{w}^H(t) \mathbf{h}_L(\mathbf{c}, t)|^2}{\sigma_L^2}, \quad \gamma_{E,m}(\mathbf{c}, \mathbf{w}(t), t) = \frac{|\mathbf{w}^H(t) \mathbf{h}_{E,m}(\mathbf{c}, t)|^2}{\sigma_{E,m}^2}. \quad (20)$$

where σ_L^2 and $\sigma_{E,m}^2$ denote the noise powers at S_L and $S_{E,m}$, respectively. Based on the above, the instantaneous secrecy rate at time t is written as

$$C_s(\mathbf{c}, \mathbf{w}(t), t) = \left[\log_2(1 + \gamma_L(\mathbf{c}, \mathbf{w}(t), t)) - \max_{m \in \mathcal{M}} \log_2(1 + \gamma_{E,m}(\mathbf{c}, \mathbf{w}(t), t)) \right]^+, \quad (21)$$

where $[x]^+ \triangleq \max\{x, 0\}$ denotes the nonnegative part of x .

2.3 Problem Formulation

Satellites in the same orbital plane travel along the same trajectory, with differences only in their phase offsets. Hence, the evolution of each orbital plane can be represented by tracking one representative satellite. Meanwhile, due to the Earth's rotation, the relative geometry between the GS and the satellite constellation varies periodically over time. To capture the periodic variation of the satellite-ground geometry, we consider a representative observation interval with duration \bar{T} . Specifically, since the J orbital planes are uniformly distributed in azimuth, the same spatial geometry recurs when the Earth rotates by an angular interval of $2\pi/J$. Accordingly, the observation interval is given by $\bar{T} = T_E/J$. For analytical consistency, \bar{T} is chosen as an integer multiple of T/K , which guarantees the alignment of time slots among different orbital planes. The observation interval is then uniformly divided into P time slots of equal duration. The midpoint of the p -th time slot is defined as $t_p = (p - \frac{1}{2})\bar{T}/P$, where $p \in \mathcal{P} \triangleq \{1, \dots, P\}$. To avoid excessive mechanical overhead, the antenna position vector is assumed to remain fixed over all time slots and thus does not depend on the time-slot index after discretization. The legitimate SNR and the m -th eavesdropping SNR in the p -th slot are defined as

$$\gamma_L(\mathbf{c}, \mathbf{w}[p], t_p) = \frac{|\mathbf{w}^H[p] \mathbf{h}_L(\mathbf{c}, t_p)|^2}{\sigma_L^2}, \quad \gamma_{E,m}(\mathbf{c}, \mathbf{w}[p], t_p) = \frac{|\mathbf{w}^H[p] \mathbf{h}_{E,m}(\mathbf{c}, t_p)|^2}{\sigma_{E,m}^2}. \quad (22)$$

The achievable rates of the legitimate and the m -th eavesdropping LEO satellite are defined as

$$A_L(\mathbf{c}, \mathbf{w}[p], t_p) = \log_2(1 + \gamma_L(\mathbf{c}, \mathbf{w}[p], t_p)), \quad A_{E,m}(\mathbf{c}, \mathbf{w}[p], t_p) = \log_2(1 + \gamma_{E,m}(\mathbf{c}, \mathbf{w}[p], t_p)). \quad (23)$$

1) In each time slot, the GS communicates with only one authorized LEO satellite, while all the other visible satellites are treated as potential eavesdroppers. Due to the high mobility of LEO satellites, the serving satellite may change over time to maintain service continuity. Such a handover only updates the legitimate receiver and does not imply information leakage.

Accordingly, the instantaneous secrecy rate in the p -th slot is given by

$$C_s(\mathbf{c}, \mathbf{w}[p], t_p) = [A_L(\mathbf{c}, \mathbf{w}[p], t_p) - \max_{m \in \mathcal{M}} A_{E,m}(\mathbf{c}, \mathbf{w}[p], t_p)]^+. \quad (24)$$

The average secrecy rate over $(0, \bar{T}]$ can be approximated by the mean of the per-slot secrecy rates

$$\bar{C}_s(\mathbf{c}, \mathbf{w}[p]) \approx \frac{1}{P} \sum_{p=1}^P C_s(\mathbf{c}, \mathbf{w}[p], t_p). \quad (25)$$

The objective is to maximize the average secrecy rate of the considered uplink system through the joint optimization of the transmit beamforming vector and the MA position vector, subject to the per-element movement region constraints, the GS transmit power constraint, and the minimum secrecy rate requirement. Accordingly, the resulting optimization problem is formulated as

$$(P1) : \quad \max_{\mathbf{c}, \{\mathbf{w}[p]\}_{p=1}^P} \bar{C}_s(\mathbf{c}, \mathbf{w}[p]) \quad (26a)$$

$$\text{s.t.} \quad C_s(\mathbf{c}, \mathbf{w}[p], t_p) \geq C_{\min}, \quad (26b)$$

$$\|\mathbf{w}[p]\|_2^2 \leq P_{\max}, \quad (26c)$$

$$\mathbf{c}_n \in \mathcal{C}, \quad (26d)$$

$$\|\mathbf{c}_n - \mathbf{c}_{\tilde{n}}\|_2 \geq d_{\min}, \quad (26e)$$

$$\forall n, \tilde{n} \in \mathcal{N}, n \neq \tilde{n}, \quad (26f)$$

where C_{\min} denotes the minimum required secrecy rate. P_{\max} denotes the maximum power budget. d_{\min} represents the minimum allowable distance between any two antenna elements. Constraint (26b) is the minimum secrecy rate constraint for each time slot of the proposed system. Constraint (26c) is minimum power constraint. Constraint (26d) characterizes the allowable movement region of the antennas, and constraint (26e) enforces a minimum inter-antenna separation constraint with threshold d_{\min} . We can note that (P1) is non-convex. The non-convexity mainly stems from the following reasons: 1) the objective function involves a max operation, and $\{\mathbf{w}[p]\}_{p=1}^P$ is highly coupled with \mathbf{c} ; 2) constraint (26b) includes the secrecy rate is non-convex; and 3) the feasible set defined by constraint (26e) is non-convex.

3 Proposed SCA-Based AO Algorithm

To address the above problem, an AO method is proposed, where the MA position and beamforming vectors are updated alternately. Specifically, the $\{\mathbf{w}[p]\}_{p=1}^P$ are optimized with the \mathbf{c} fixed, while the \mathbf{c} is optimized with fixed $\{\mathbf{w}[p]\}_{p=1}^P$.

3.1 Optimization of $\{\mathbf{w}[p]\}_{p=1}^P$ with Fixed \mathbf{c}

Firstly, reformulate (P1) into a more manageable form. Let $A_E(\mathbf{c}, \mathbf{w}[p], t_p) = \max_{m \in \mathcal{M}} A_{E,m}(\mathbf{c}, \mathbf{w}[p], t_p)$. Introduce non-negative auxiliary variables $\tau[p] \geq 0$ and $r_E[p]$

$$\tau[p] \leq A_L(\mathbf{c}, \mathbf{w}[p], t_p) - r_E[p], \quad A_{E,m}(\mathbf{c}, \mathbf{w}[p], t_p) \leq r_E[p], \quad \forall m. \quad (27)$$

In the original problem, the transmit beamforming vector is rewritten as

$$\mathbf{W}[p] = \mathbf{w}[p] \mathbf{w}[p]^H. \quad (28)$$

We define

$$\mathbf{S}_L(\tilde{\mathbf{b}}_L(t_p), \mathbf{c}) = \rho_L(t_p) \mathbf{s}_L(\tilde{\mathbf{b}}_L(t_p), \mathbf{c}) \mathbf{s}_L(\tilde{\mathbf{b}}_L(t_p), \mathbf{c})^H, \quad (29)$$

$$\mathbf{S}_{E,m}(\tilde{\mathbf{b}}_{E,m}(t_p), \mathbf{c}) = \rho_{E,m}(t_p) \mathbf{s}_{E,m}(\tilde{\mathbf{b}}_{E,m}(t_p), \mathbf{c}) \mathbf{s}_{E,m}(\tilde{\mathbf{b}}_{E,m}(t_p), \mathbf{c})^H. \quad (30)$$

The transformed matrix must satisfy $\text{rank}(\mathbf{W}[p]) = 1, \forall p \in \mathcal{P}$. Therefore, the optimization problem can be rewritten as

$$(P2) : \max_{\{\mathbf{W}[p]\}_{p=1}^P, \{\tau[p]\}_{p=1}^P, \{r_E[p]\}_{p=1}^P} \frac{1}{P} \sum_{p=1}^P \tau[p] \quad (31a)$$

$$\text{s.t. } \tau[p] \geq C_{\min}, \quad (31b)$$

$$\log_2\left(1 + \frac{\text{Tr}(\mathbf{S}_L(\tilde{\mathbf{b}}_L(t_p), \mathbf{c})\mathbf{W}[p])}{\sigma_L^2}\right) \geq \tau[p] + r_E[p], \quad (31c)$$

$$\log_2\left(1 + \frac{\text{Tr}(\mathbf{S}_{E,m}(\tilde{\mathbf{b}}_{E,m}(t_p), \mathbf{c})\mathbf{W}[p])}{\sigma_{E,m}^2}\right) \leq r_E[p], \quad (31d)$$

$$\text{Tr}(\mathbf{W}[p]) \leq P_{\max}, \quad (31e)$$

$$\text{rank}(\mathbf{W}[p]) = 1, \quad (31f)$$

$$\mathbf{W}[p] \succeq \mathbf{0}. \quad (31g)$$

Owing to its non-convexity, (P2) is intractable to solve directly. This is mainly because constraint (31d) is in the form of a concave function being upper-bounded by a linear function, which leads to a non-convex feasible region. In addition, constraint (31f) is also non-convex.

With \mathbf{c} fixed, (P2) can be reformulated as a semidefinite program (SDP)

$$(P3) : \max_{\{\mathbf{W}[p]\}_{p=1}^P, \{\tau[p]\}_{p=1}^P, \{r_E[p]\}_{p=1}^P} \frac{1}{P} \sum_{p=1}^P \tau[p] \quad (32a)$$

$$\text{s.t. (31b) - (31e), (31g)}. \quad (32b)$$

Note that the rank-one constraint in (31f) is temporarily relaxed to obtain a SDP. Constraint (31d) in (P3) has non-convex characteristics and are difficult to solve directly. Define

$$f_{E,m}(\mathbf{W}[p]) \triangleq \log_2\left(1 + \frac{\text{Tr}(\mathbf{S}_{E,m}(p)\mathbf{W}[p])}{\sigma_{E,m}^2}\right). \quad (33)$$

Since $f_{E,m}(\mathbf{W}[p])$ is concave in $\mathbf{W}[p]$, its first-order Taylor expansion at $\mathbf{W}^{(0)}[p]$ serves as a global upper bound

$$f_{E,m}(\mathbf{W}[p]) \leq f_{E,m}(\mathbf{W}^{(0)}[p]) + \frac{1}{\ln 2} \frac{\text{Tr}(\mathbf{S}_{E,m}(p)(\mathbf{W}[p] - \mathbf{W}^{(0)}[p]))}{\sigma_{E,m}^2 + \text{Tr}(\mathbf{S}_{E,m}(p)\mathbf{W}^{(0)}[p])}. \quad (34)$$

After the above transformation, constraint (31d) is recast into a convex form. Then, (P3) can be efficiently solved via CVX [32]. If the solution obtained from SDR fails to satisfy the rank-one constraint, the Gaussian randomization technique can be applied to generate a feasible rank-one solution based on the CVX output. Specifically, the suboptimal solution $\{\bar{\mathbf{W}}[p]\}_{p=1}^P$ is first decomposed by eigenvalue decomposition (EVD) as

$$\bar{\mathbf{W}}[p] = \mathbf{U}_p \Sigma_p \mathbf{U}_p^H, \quad (35)$$

where $\mathbf{U}_p \in \mathbb{C}^{N \times N}$ and $\Sigma_p \in \mathbb{C}^{N \times N}$ denote the eigenvector matrix and the diagonal matrix of eigenvalues, respectively. Generate an approximate solution based on the Jordan matrix and the diagonal matrix

$$\tilde{\mathbf{w}}[p] = \sqrt{P_{\max}} \frac{\mathbf{U}_p \Sigma_p^{1/2} \mathbf{R}}{\left\| \mathbf{U}_p \Sigma_p^{1/2} \mathbf{R} \right\|_2}, \quad (36)$$

where $\mathbf{R} \sim \mathcal{CN}(0, \mathbf{I}_N)$ is random vector. Multiple randomization trials are performed, and the one yielding the largest objective value is selected. Finally, the high-precision solution of the original problem is restored.

3.2 Optimization of \mathbf{c} with Fixed $\{\mathbf{w}[p]\}_{p=1}^P$

When fixed $\{\mathbf{w}[p]\}_{p=1}^P$, (P1) can be reformulated as

$$(P4) : \max_{\mathbf{c}} \bar{C}_s(\mathbf{c}) \quad (37a)$$

$$\text{s.t.}(26b), (26d), (26e), (26f). \quad (37b)$$

(P4) is non-convex due to the constraints (26b) and (26e). As a result, standard convex optimization methods cannot be directly applied. We adopt an SCA framework to solve (P4), where the non-convex parts are iteratively approximated via first-order Taylor expansions around the current iterate.

First, to address the non-smooth maximum operation involved in the eavesdroppers' achievable rate, the log-sum-exp function is adopted as a smooth approximation. Specifically, the maximum eavesdropping rate is approximated as

$$\tilde{A}_E(\mathbf{c}, t_p) = \mu \ln \left(\sum_{m \in \mathcal{M}} e^{A_{E,m}(\mathbf{c}, t_p)/\mu} \right), \quad (38)$$

where $\mu > 0$ is a smoothing parameter. As $\mu \rightarrow 0$, the above expression approaches the maximum function. Accordingly, the objective function can be reformulated as

$$\tilde{C}_s(\mathbf{c}) = \frac{1}{P} \sum_{p=1}^P A_L(\mathbf{c}, t_p) - \tilde{A}_E(\mathbf{c}, t_p). \quad (39)$$

A global lower bound of the objective function is obtained via the first-order Taylor expansion at the current point $\mathbf{c}^{(r)}$

$$\tilde{C}_s(\mathbf{c}) \geq \tilde{C}_s(\mathbf{c}^{(r)}) + \nabla_{\mathbf{c}} \tilde{C}_s(\mathbf{c}^{(r)})^T (\mathbf{c} - \mathbf{c}^{(r)}). \quad (40)$$

We next derive the gradients of $A_L(\mathbf{c}, t_p)$ and $\tilde{A}_E(\mathbf{c}, t_p)$ with respect to variable \mathbf{c} .

For any channel $\chi \in \{L, E, m\}$ and time slot p , the SNR is defined as

$$\gamma_\chi(\mathbf{c}, t_p) = \frac{|\mathbf{w}[p]^H \mathbf{h}_\chi(\mathbf{c}, t_p)|^2}{\sigma_\chi^2}. \quad (41)$$

According to the system model, after fixing $\{\mathbf{w}[p]\}_{p=1}^P$, the received signal power can be written as

$$\left| \mathbf{w}[p]^H \mathbf{h}_\chi(\mathbf{c}, t_p) \right|^2 = \rho_\chi(t_p) \mathbf{s}_\chi(\tilde{\mathbf{b}}_\chi(t_p), \mathbf{c})^H \mathbf{W}[p] \mathbf{s}_\chi(\tilde{\mathbf{b}}_\chi(t_p), \mathbf{c}), \quad (42)$$

where $\mathbf{W}[p] = \mathbf{w}[p] \mathbf{w}[p]^H$. To simplify subsequent derivations, we define

$$u_\chi(\mathbf{c}, t_p) = \mathbf{s}_\chi^H(\tilde{\mathbf{b}}_\chi(t_p), \mathbf{c}) \mathbf{W}[p] \mathbf{s}_\chi(\tilde{\mathbf{b}}_\chi(t_p), \mathbf{c}), \quad a_\chi(t_p) = \frac{\rho_\chi(t_p)}{\sigma_\chi^2}. \quad (43)$$

Accordingly, the SNR can be compactly written as

$$\gamma_\chi(\mathbf{c}, t_p) = a_\chi(t_p) u_\chi(\mathbf{c}, t_p). \quad (44)$$

Derive the gradient of the achievable rate $A_\chi(\mathbf{c}, t_p)$ with respect to the MA position vector of the n -th antenna element, \mathbf{c}_n . By applying the chain rule, we have

$$\frac{\partial A_\chi(\mathbf{c}, t_p)}{\partial \mathbf{c}_n} = \frac{1}{\ln 2} \frac{1}{1 + \gamma_\chi(\mathbf{c}, t_p)} a_\chi(t_p) \frac{\partial u_\chi(\mathbf{c}, t_p)}{\partial \mathbf{c}_n}. \quad (45)$$

The steering vector towards satellite χ of n -th antenna element in MA array can be expressed as

$$\mathbf{s}_{\chi,n} = e^{j\varphi_{\chi,n}(t_p)}, \quad (46)$$

where $\varphi_{\chi,n}(t_p) = \mathbf{k}_\chi(t_p)^T \mathbf{c}_n$, and $\mathbf{k}_\chi(t_p)$ denotes the horizontal component of the normalized wave vector $\tilde{\mathbf{b}}_\chi(t_p)$. Taking the derivative with respect to \mathbf{c}_n yields

$$\frac{\partial \mathbf{s}_{\chi,n}}{\partial \mathbf{c}_n} = j e^{j\varphi_{\chi,n}(t_p)} \mathbf{k}_\chi(t_p) = j \mathbf{s}_{\chi,n} \mathbf{k}_\chi(t_p), \quad (47)$$

and similarly

$$\frac{\partial \mathbf{s}_{\chi,n}^H}{\partial \mathbf{c}_n} = -j \mathbf{s}_{\chi,n}^H \mathbf{k}_\chi(t_p). \quad (48)$$

The received signal power can be expressed as the quadratic form

$$u_\chi(\mathbf{c}, t_p) = \sum_{i=1}^N \sum_{j=1}^N \mathbf{s}_{\chi,n}^H \mathbf{W}_{i,j}[p] \mathbf{s}_{\chi,j}. \quad (49)$$

It can be observed that the gradient with respect to \mathbf{c}_n only involves the n -th row and column of $\mathbf{W}[p]$. After straightforward algebraic manipulation, the gradient of $u_\chi(\mathbf{c}, t_p)$ with respect to variable \mathbf{c}_n is obtained as

$$\frac{\partial u_\chi(\mathbf{c}, t_p)}{\partial \mathbf{c}_n} = 2 \text{Im} \{ \mathbf{s}_{\chi,n}^H (\mathbf{W}[p] \mathbf{s}_\chi)_n \} \mathbf{k}_\chi(t_p). \quad (50)$$

Using the chain rule, the gradient of the smoothed eavesdropping achievable rate with respect to \mathbf{c} can be expressed as

$$\nabla_{\mathbf{c}} \tilde{A}_E(\mathbf{c}, t_p) = \sum_{m \in \mathcal{M}} \frac{e^{A_{E,m}(\mathbf{c}, t_p)/\mu}}{\sum_{i \in \mathcal{M}} e^{A_{E,i}(\mathbf{c}, t_p)/\mu}} \nabla_{\mathbf{c}} A_{E,m}(\mathbf{c}, t_p). \quad (51)$$

According to (50) and (51), the complete gradient expression of the objective function is provided at the bottom of this page.

According (52), non-convex constraint (26b) can be rewritten as

$$A_L(\mathbf{c}^{(r)}, t_p) - \tilde{A}_E(\mathbf{c}^{(r)}, t_p) + \nabla_{\mathbf{c}}(A_L(\mathbf{c}^{(r)}, t_p) - \tilde{A}_E(\mathbf{c}^{(r)}, t_p))^T (\mathbf{c} - \mathbf{c}^{(r)}) \geq C_{\min}. \quad (53)$$

Constraint (26e) is non-convex. Noting that the Euclidean norm is a convex function, a first-order Taylor expansion at the current point $\mathbf{c}^{(r)}$ yields a global lower bound, which leads to the following linear constraint

$$\frac{(\mathbf{c}_n^{(r)} - \mathbf{c}_{\tilde{n}}^{(r)})^T}{\|\mathbf{c}_n^{(r)} - \mathbf{c}_{\tilde{n}}^{(r)}\|_2} (\mathbf{c}_n - \mathbf{c}_{\tilde{n}}) \geq d_{\min}, \quad \forall n \neq \tilde{n}. \quad (54)$$

Based on the above smoothing and gradient derivations, (P4) can be rewritten as the following problem

$$(P5) : \max_{\mathbf{c}} \tilde{C}_s(\mathbf{c}^{(r)}, t_p) + \nabla_{\mathbf{c}} \tilde{C}_s(\mathbf{c}^{(r)}, t_p)^T (\mathbf{c} - \mathbf{c}^{(r)}) \quad (55a)$$

$$\text{s.t.} \quad (53), (54), (26d), (26f). \quad (55b)$$

All the non-convex components in (P4) have been equivalently transformed into convex forms. As a result, (P5) can be recast as a convex optimization problem and thus solved efficiently by employing the interior-point method.

3.3 The Convergence and Computational Complexity

We propose an SCA-based AO algorithm to update the variables $\{\mathbf{w}[p]\}_{p=1}^P$ and \mathbf{c} . For each subproblem, the non-convex terms are replaced by their first-order surrogate functions, which are constructed to be locally tight at the current iterate and satisfy the required low bound. As a result, solving each subproblem yields a feasible solution that does not decrease the original objective value. Therefore, the objective value generated by the outer AO iterations is monotonically non-decreasing. Moreover, under the finite transmit power constraint and the bounded logarithmic rate function, the achievable secrecy rate is upper bounded. Therefore, the objective value is guaranteed

$$\begin{aligned} \nabla_{\mathbf{c}} \tilde{C}_s(\mathbf{c}) = & \frac{1}{P} \sum_{p=1}^P \left[\frac{2a_L(t_p)}{\ln 2(1 + a_L(t_p)u_L(\mathbf{c}, t_p))} \text{Im} \{ s_{L,n}(\mathbf{c}, t_p)^H (\mathbf{W}[p] \mathbf{s}_L(\mathbf{c}, t_p))_n \} \mathbf{k}_L(t_p) \right. \\ & \left. - \sum_{m \in \mathcal{M}} \frac{e^{A_{E,m}(\mathbf{c}, t_p)/\mu}}{\sum_{i \in \mathcal{M}} e^{A_{E,i}(\mathbf{c}, t_p)/\mu}} \frac{2a_{E,m}(t_p)}{\ln 2(1 + a_{E,m}(t_p)u_{E,m}(\mathbf{c}, t_p))} \text{Im} \{ s_{E,m,n}(\mathbf{c}, t_p)^H (\mathbf{W}[p] \mathbf{s}_{E,m}(\mathbf{c}, t_p))_n \} \mathbf{k}_{E,m}(t_p) \right]. \end{aligned} \quad (52)$$

Algorithm 1 SCA-Based AO Algorithm for Solving (P1)

- 1: **Initialize:** Set $r = 0$, and choose feasible $\mathbf{c}^{(0)}$ and $\{\mathbf{w}^{(0)}[p]\}_{p=1}^P$.
 - 2: **repeat**
 - 3: Given $\mathbf{c}^{(r)}$, solve (P3) via SDR to obtain $\{\mathbf{W}^{(r+1)}[p]\}_{p=1}^P$.
 - 4: Recover $\{\mathbf{w}^{(r+1)}[p]\}_{p=1}^P$ from $\{\mathbf{W}^{(r+1)}[p]\}_{p=1}^P$ via Gaussian randomization.
 - 5: Given $\{\mathbf{w}^{(r+1)}[p]\}_{p=1}^P$, solve (P5) to obtain $\mathbf{c}^{(r+1)}$.
 - 6: Set $r = r + 1$.
 - 7: **until** convergence
 - 8: **Output:** $\mathbf{c}^* = \mathbf{c}^{(r)}$ and $\{\mathbf{w}^*[p]\}_{p=1}^P = \{\mathbf{w}^{(r)}[p]\}_{p=1}^P$.
-

to converge. According to the standard convergence conditions of SCA, the proposed SCA-based AO algorithm converges to a local optimum of the original non-convex problem. The overall procedure of the proposed algorithm is summarized in **Algorithm 1**.

For the SCA-based AO algorithm, the beamforming update in each outer iteration requires solving P independent SDP subproblems, each with an $N \times N$ positive semidefinite matrix variable. The complexity under an interior-point method is $\mathcal{O}(I_W P N^6)$, where I_W denotes the number of SCA iterations for the beamforming subproblem. For the antenna position update, the SCA reformulation leads to a linear program with $2N$ variables and $(N + \frac{N(N-1)}{2})$ linear constraints, whose complexity is $\mathcal{O}(I_C \times (N + \frac{N(N-1)}{2}) \times (2N)^3)$, where I_C is the number of SCA iterations for updating \mathbf{c} . Therefore, the total complexity of the SCA-based AO algorithm can be approximated as

$$\mathcal{O}(I_{\text{AO}}(I_W P N^6 + (I_C \times (N + \frac{N(N-1)}{2}) \times (2N)^3))), \quad (56)$$

where I_{AO} denotes the number of outer AO iterations.

4 Proposed DE-Based AO Algorithm

In this section, we employ a DE-based AO algorithm to solve (P1). Although the SCA-based AO algorithm has a clear mathematical structure and can obtain relatively accurate solutions to each approximated subproblem, it obtains local optimization through SCA. Hence, its performance may still depend on the initialization and the approximation quality, especially for the highly non-convex MA position vector subproblem with strongly coupled spacing constraints. Motivated by this, we further propose a DE-based AO algorithm. As a derivative-free population-based search method, DE does not rely on gradient information or local convexification, and thus is more suitable for exploring complicated non-convex feasible regions. Therefore, compared with the SCA-based method, the DE-based approach offers stronger global exploration capability and serves as a complementary solution for antenna position optimization.

4.1 DE Algorithm for Antenna Position Optimization

In the proposed DE-based AO algorithm, the beamforming subproblem is still solved by the SDR-based method developed in the previous section, while the MA position vector subproblem is handled by DE algorithm. DE is a stochastic optimization method that iteratively evolves a population of candidate solutions over G_{max} generations [33]. Specifically, the algorithm begins with a randomly generated population of N_{pop} individuals within the feasible search space, defined as

$$\mathcal{P}^{(0)} = \left\{ \mathbf{c}_1^T, \mathbf{c}_2^T, \dots, \mathbf{c}_{N_{\text{pop}}}^T \right\}. \quad (57)$$

After initialization, the best individual in the population is recorded as the elite solution

$$\mathbf{c}_{\text{elite}}^{(0)} = \arg \max_{\mathbf{c}_i \in \mathcal{P}^{(0)}} \mathcal{F}(\mathbf{c}_i), \quad (58)$$

where $\mathbf{c}_{\text{elite}}^{(0)}$ denotes the elite individual in the initial population. Then, in each generation $g = 0, 1, \dots, G_{\text{max}} - 1$, DE produces trial individuals through mutation and crossover operations, followed by greedy selection according to their fitness values. The specific operation is as follows

- **Mutation:** Randomly select three different individuals $\mathbf{c}_{r_1}, \mathbf{c}_{r_2}, \mathbf{c}_{r_3}$ to perform the mutation operation

$$\mathbf{v}_i = \mathbf{c}_{r_1} + F(\mathbf{c}_{r_2} - \mathbf{c}_{r_3}), \quad (59)$$

where $i \in \mathcal{N}_{\text{pop}} = \{1, 2, \dots, N_{\text{pop}}\}$, and F denotes scale factor.

• **Crossover:** A trial vector \mathbf{u}_i is obtained by performing crossover between the mutated vector \mathbf{v}_i and \mathbf{c}_i . Set the k -th dimension component to

$$[\mathbf{u}_i]_k = \begin{cases} [\mathbf{v}_i]_k, & \text{if } \bar{k} < C_R \text{ or } k = \tilde{k}, \\ [\mathbf{c}_i]_k, & \text{otherwise,} \end{cases} \quad (60)$$

where $\bar{k} \sim \mathcal{U}(0, 1)$ denotes the uniform random variable. C_R is the crossover control parameter. \tilde{k} represents the random index that must inherit at least one variant component by default. After the crossover operation, the trial vector \mathbf{u}_i may violate the antenna movement region and the minimum inter-antenna spacing constraints. Therefore, a feasibility repair procedure is applied before fitness evaluation. Each element of \mathbf{u}_i is first projected onto the feasible movement region defined in (26d). Specifically, for the k -th component, we have

$$[\mathbf{u}_i]_k \leftarrow \min \{ \max \{ [\mathbf{u}_i]_k, l_k \}, u_k \}, \quad (61)$$

where l_k and u_k denote the lower and upper limits of the k -th coordinate, respectively. If constraint (26e) is violated, their positions are symmetrically adjusted along the separating direction

$$\mathbf{c}_n \leftarrow \mathbf{c}_n + \frac{\Delta_{n\bar{n}}}{2} \mathbf{d}_{n\bar{n}}, \mathbf{c}_{\bar{n}} \leftarrow \mathbf{c}_{\bar{n}} - \frac{\Delta_{n\bar{n}}}{2} \mathbf{d}_{n\bar{n}}, \quad (62)$$

$$\mathbf{d}_{n\bar{n}} = \frac{\mathbf{c}_n - \mathbf{c}_{\bar{n}}}{\|\mathbf{c}_n - \mathbf{c}_{\bar{n}}\|_2}, \Delta_{n\bar{n}} = d_{\min} - \|\mathbf{c}_n - \mathbf{c}_{\bar{n}}\|_2. \quad (63)$$

This adjustment is iteratively applied to all violating antenna pairs until all spacing constraints are satisfied.

• **Selection:** This stage selects the candidate with superior fitness for inclusion in the next iteration. Specifically, the selection procedure is defined as follows

$$\mathbf{c}_i = \begin{cases} \mathbf{u}_i, & \text{if } \mathcal{F}(\mathbf{u}_i) \geq \mathcal{F}(\mathbf{c}_i), \\ \mathbf{c}_i, & \text{otherwise.} \end{cases} \quad (64)$$

In addition, an elitism strategy is adopted to preserve the best-so-far solution

$$\mathbf{c}_{elite}^{(g+1)} = \arg \max_{\mathbf{c}_i \in \mathcal{P}^{(g+1)} \cup \{\mathbf{c}_{elite}^{(g)}\}} \mathcal{F}(\mathbf{c}_i). \quad (65)$$

After the greedy selection, the elite individual is updated by comparing the current population with the elite solution from the previous generation. Then, the updated elite individual is forcibly retained in the next generation to prevent the loss of the best solution found so far. Without loss of generality, the elite individual is inserted into the next generation by replacing the first individual in the population.

4.2 The Convergence and Computational Complexity

For the DE-based AO algorithm, the beamforming subproblem is still solved optimally with fixed antenna positions, while the antenna position subproblem is handled by DE. In each outer iteration, the DE procedure is designed to retain the best feasible individual, and the antenna position update is accepted only when it does not decrease the objective value. Consequently, the objective value generated by the outer AO iterations is also monotonically non-decreasing. Since the achievable secrecy rate is limited by the transmit power and the bounded $\log(1 + \text{SNR})$ function, this objective value must converge. Nevertheless, because DE is a population-based heuristic search method, it is generally difficult to establish the stationary-point convergence of the overall algorithm in a strict sense. As a result, the objective value of the DE-based AO algorithm is guaranteed to converge, and the final solution is a feasible local optimum for the original problem. The detailed steps of the proposed algorithm are provided in **Algorithm 2**.

For the DE-based AO algorithm, the beamforming update has the same complexity $\mathcal{O}(I_W P N^6)$. The difference lies in the antenna position update, which is performed by DE. For a population size N_{pop} and G_{\max} generations, the dominant cost comes from the fitness evaluations of all individuals, resulting in a complexity of $\mathcal{O}(G_{\max} N_{\text{pop}} P M N)$, where M denotes the number of eavesdropping satellites per time slot. Therefore, the total complexity of the DE-based AO algorithm can be approximated as

$$\mathcal{O}(T_{\max} (I_W P N^6 + G_{\max} N_{\text{pop}} (P M N))). \quad (66)$$

Algorithm 2 DE-Based AO Algorithm for Solving (P1)

```

1: Initialize: Set  $r = 0$ , and choose feasible  $\mathbf{c}^{(0)}$  and  $\{\mathbf{w}^{(0)}[p]\}_{p=1}^P$ . Set  $F$ ,  $C_R$ ,  $N_{\text{pop}}$ ,  $G_{\text{max}}$ , and  $T_{\text{max}}$ .
2: repeat
3:   Given  $\mathbf{c}^{(r)}$ , solve (P3) to obtain  $\{\mathbf{w}^{(r+1)}[p]\}_{p=1}^P$ .
4:   Set  $g = 0$  and initialize  $\mathcal{P}^{(g)} = \{\mathbf{c}_i^{(g)}\}_{i=1}^{N_{\text{pop}}}$  based on  $\mathbf{c}^{(r)}$ .
5:   Repair all individuals by (61)–(63) and compute their fitness values  $\mathcal{F}(\mathbf{c}_i^{(g)})$ .
6:   Set  $\mathbf{c}_{\text{elite}}^{(g)} = \arg \max_{\mathbf{c}_i^{(g)} \in \mathcal{P}^{(g)}} \mathcal{F}(\mathbf{c}_i^{(g)})$ .
7:   repeat
8:     for  $i = 1$  to  $N_{\text{pop}}$  do
9:       Randomly select  $r_1, r_2$ , and  $r_3$ , where  $r_1, r_2, r_3 \neq i$ .
10:      Mutation:  $\mathbf{v}_i^{(g)} = \mathbf{c}_{r_1}^{(g)} + F(\mathbf{c}_{r_2}^{(g)} - \mathbf{c}_{r_3}^{(g)})$ .
11:      Crossover: Generate  $\mathbf{u}_i^{(g)}$  from  $\mathbf{v}_i^{(g)}$  and  $\mathbf{c}_i^{(g)}$  with rate  $C_R$ .
12:      Repair  $\mathbf{u}_i^{(g)}$  by projecting it onto the movement region using (61).
13:      If the spacing constraints are violated, adjust the violating antenna pairs by (62)–(63).
14:      Evaluate  $\mathbf{u}_i^{(g)}$  by computing  $\mathcal{F}(\mathbf{u}_i^{(g)})$ .
15:      if  $\mathcal{F}(\mathbf{u}_i^{(g)}) \geq \mathcal{F}(\mathbf{c}_i^{(g)})$  then
16:         $\mathbf{c}_i^{(g+1)} = \mathbf{u}_i^{(g)}$ .
17:      else
18:         $\mathbf{c}_i^{(g+1)} = \mathbf{c}_i^{(g)}$ .
19:      end if
20:    end for
21:    Update  $\mathbf{c}_{\text{elite}}^{(g+1)} = \arg \max_{\mathbf{c} \in \mathcal{P}^{(g+1)} \cup \{\mathbf{c}_{\text{elite}}^{(g)}\}} \mathcal{F}(\mathbf{c})$ .
22:    Replace the first individual in  $\mathcal{P}^{(g+1)}$  with  $\mathbf{c}_{\text{elite}}^{(g+1)}$ .
23:    Set  $g = g + 1$ .
24:  until  $g = G_{\text{max}}$ 
25:  Set  $\mathbf{c}^{(r+1)}$  as the best individual in  $\mathcal{P}^{(G_{\text{max}})}$ .
26:  Set  $r = r + 1$ .
27: until  $r = T_{\text{max}}$ 
28: Output:  $\mathbf{c}^* = \mathbf{c}^{(r)}$  and  $\{\mathbf{w}^*[p]\}_{p=1}^P = \{\mathbf{w}^{(r)}[p]\}_{p=1}^P$ .

```

5 Numerical Results

This section provides a comprehensive simulation-based evaluation of the proposed system and the developed algorithms. Unless otherwise specified, the system operates at 12 GHz. The LEO satellites are deployed at an altitude of 550 km, with the Earth radius set to 6371 km and the orbital inclination angle set to 50° . The minimum inter-element spacing of the MA array $d_{\min} = 0.5\lambda$, and the move region of MA $\mathcal{C} = 3\lambda \times 3\lambda$. The GS transmit power is 40 dBm, and the noise power is -148 dBm. The minimum required secrecy rate $C_{\min} = 0.01$ (bit/s/Hz). The path loss exponent $\alpha = 2$. The smoothing parameter $\mu = 0.05$. The maximum iteration number of DE-based AO algorithm $T_{\text{max}} = 100$, the population size $N_{\text{pop}} = 50$, the scale factor $F = 0.9$, and the crossover control parameter $C_R = 0.9$. To facilitate a clear and fair comparison, the following benchmark schemes are adopted: 1) **SCA-AO** refers to the AO algorithm in which the antenna position subproblem is solved using the SCA method; 2) **DE-AO** refers to the AO algorithm in which the antenna position subproblem is solved using the DE method; 3) **FPA** refers to fixing the antenna positions and only optimizing the beamforming.

Fig. 3 illustrates the convergence behavior of the SCA-based AO algorithm under different LEO constellation configurations with a fixed number of antennas $N = 9$. It can be observed that all curves increase monotonically in the early stage and gradually converge after a certain number of iterations, which verifies the stability and effectiveness of the proposed algorithm. Moreover, as the constellation size increases, the secrecy rate decreases significantly. This is because the larger the constellation, the greater the number of visible satellites, which become potential eavesdroppers. Although a larger set of visible satellites increases the probability of connecting to a service satellite with better channel quality, it also raises the likelihood of encountering the strongest eavesdropper, leading to a decrease in the overall average secrecy rate.

Fig. 4 compares the computational complexity of the SCA-based and DE-based methods for solving the MA position optimization subproblem under different antenna numbers. It can be observed that the complexity of the SCA algorithm increases much more rapidly with N than that of the DE algorithm. This is because the SCA-based algorithm requires solving a convex optimization problem in each iteration, whose computational burden grows significantly as the number of optimization variables and spacing constraints increases with N . In contrast, the complexity of the DE-based method grows more moderately, since it mainly depends on the fitness evaluations of all individuals over multiple generations. Moreover, a larger G_{max} leads to a higher complexity for the DE-based method, while its overall growth trend remains much slower than that of the SCA-based method when N is large. These results indicate that, for the MA position optimization subproblem, the DE-based method provides better

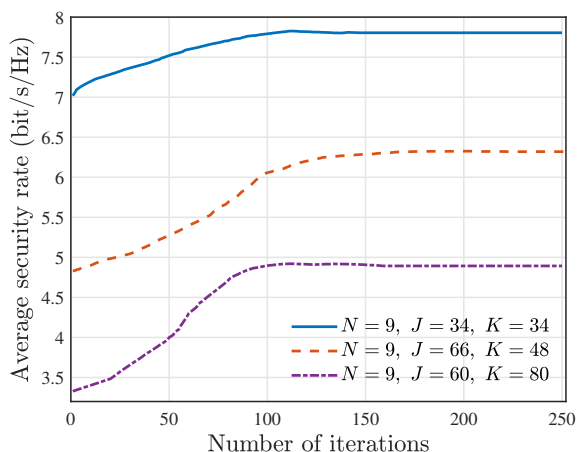


Figure 3 Convergence behavior of the proposed SCA-based AO algorithm.

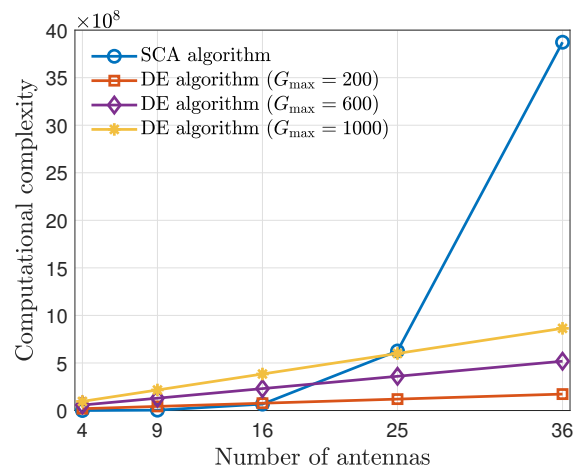
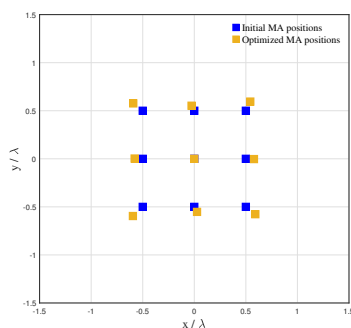
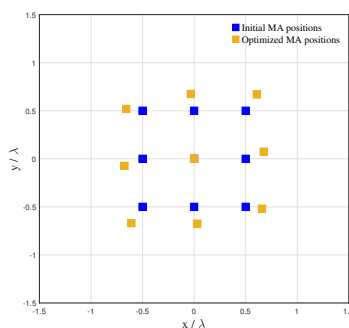


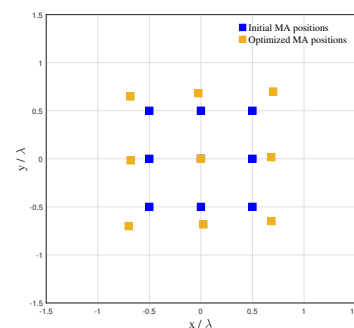
Figure 4 Complexity comparison of different algorithms.



(a) $J = 34, K = 34$



(b) $J = 66, K = 48$



(c) $J = 60, K = 80$

Figure 5 Performance comparison before and after MA antenna position optimization.

scalability than the SCA-based method as the array size increases.

In Fig. 5, we set $N = 9$, $P_{\max} = 40$ dBm. As the satellite constellation size increases, the optimized MA elements tend to move outward toward the boundary of the feasible region, resulting in an enlarged effective array aperture. This can be attributed to the increased number of satellites introduces more potential eavesdropping directions and leads to a more complex spatial interference environment. To effectively distinguish the desired satellite from multiple unintended directions, a larger aperture is required to achieve higher angular resolution and sharper beam patterns, which in turn enhances the spatial selectivity and secrecy performance of the system.

In Fig. 6, the numbers of orbital planes and satellites per plane are set to $J = 66$ and $K = 48$, respectively, while the maximum transmit power is specified as $P_{\max} = 40$ dBm. It can be observed that, as N increases, the mainlobe gain gradually becomes stronger, while the energy leaked through the sidelobes is progressively reduced. It is worth noting that the service satellite is not located exactly at the point of maximum beamforming gain. This is because, in the considered scenario with a large number of visible satellites, the MA scheme needs to strike a balance between enhancing the achievable rate of the service satellite and suppressing the achievable rates of potential eavesdropping satellites. Nevertheless, it can be clearly seen that the beamforming gains in the directions of the eavesdropping satellites are effectively suppressed to very low levels. In contrast, the FPA scheme achieves a lower beamforming gain than the proposed MA scheme, since it does not possess the additional spatial DoFs brought by antenna position optimization. Although increasing N can still improve its beam focusing capability to some extent, the resulting beam pattern remains less flexible, making it difficult to effectively suppress the gains toward the eavesdropping satellites.

Fig.7 shows the average secrecy rate versus the transmit power for different algorithms and antenna scales. It can be observed that the secrecy rate first increases and then gradually saturates as the transmit power grows. This is because, in the low-to-moderate power regime, increasing transmit power significantly enhances the legitimate channel, while at high power levels, both legitimate and eavesdropping channels are strengthened, leading to dimin-

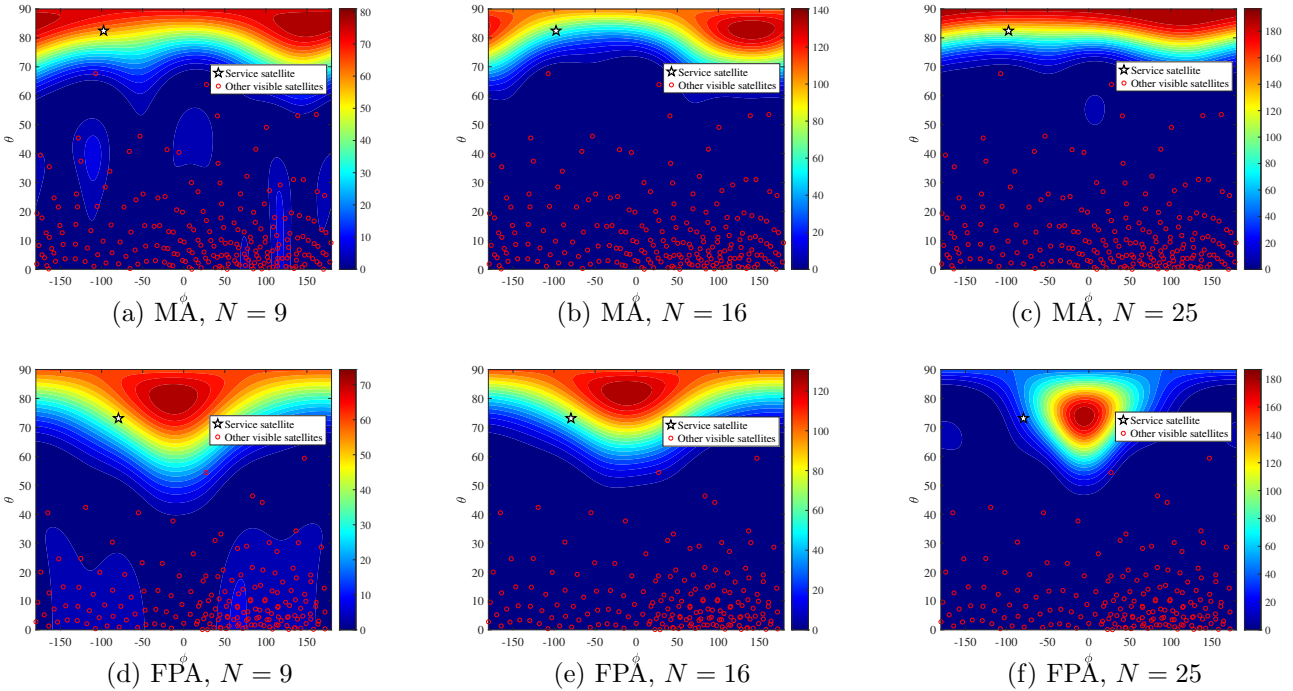


Figure 6 Beamforming gain achieved by different optimization schemes.

ishing secrecy gains. Furthermore, the MA schemes consistently outperform the FPA scheme, demonstrating that the additional spatial DoFs provided by MA position optimization can effectively enhance the legitimate channel and suppress eavesdropping channels. In particular, the proposed MA scheme achieves up to a 41% performance gain over the FPA scheme. The relative performance of SCA-based AO algorithm and DE-based AO algorithm also depends on the antenna scale. When $N = 4$, DE-based AO algorithm achieves better performance due to its global search capability in a low-dimensional space, whereas SCA-based AO algorithm is more prone to local optima. In contrast, when $N = 9$, SCA-based AO algorithm outperforms DE-based AO algorithm, as the increased problem dimension expands the search space and reduces the effectiveness of DE-based AO algorithm, while SCA-based AO algorithm better exploits local refinement. In addition, increasing the antenna number from $N = 4$ to $N = 9$ significantly improves the secrecy rate, confirming that a larger array provides higher beamforming gain and spatial resolution, thereby enhancing PLS.

In Fig. 8, we illustrate the variation of the average secrecy rate versus the number of antennas under two satellite configurations, namely $J = 66$, $K = 48$, and $J = 60$, $K = 80$. It can be observed that the average secrecy rate generally increases with the number of antennas, since more antenna elements provide higher array gain and more spatial DoFs for enhancing the legitimate channel and suppressing the eavesdropping channels. Moreover, when the number of antennas is small, the DE-based AO algorithm outperforms the SCA-based AO algorithm. This is because DE has stronger global search capability in a relatively low-dimensional feasible region, whereas SCA is more likely to be trapped in a local optimum. However, as the number of antennas increases, the SCA-based AO algorithm achieves better performance than DE-AO. The reason is that, in a higher-dimensional optimization problem, SCA can better exploit the local problem structure for refined optimization, while the search efficiency of DE gradually decreases. It is also observed that the FPA scheme consistently underperforms the MA scheme. This is because the MA scheme introduces additional spatial DoFs through MA position optimization, whereas the FPA scheme can only rely on conventional beamforming gain with fixed antenna positions.

As illustrated in Fig. 9, we set $J = 66$ and $K = 48$ to examine the effect of the GS latitude on the average secrecy rate. It is observed that both the SCA-based AO algorithm and the DE-based AO algorithm consistently outperform the conventional FPA scheme over the entire latitude range, demonstrating the superiority of MA. Moreover, for all the considered schemes, increasing the number of antenna elements from $N = 4$ to $N = 9$ yields a clear performance gain due to the enhanced spatial DoFs. It is further seen that the relative performance of the SCA-based AO algorithm and the DE-based AO algorithm varies with the array size. Specifically, when $N = 4$, the DE-based AO algorithm performs better than the SCA-based AO algorithm because its global search is more effective in a low-dimensional space. By contrast, when $N = 9$, the SCA-based AO algorithm achieves a higher

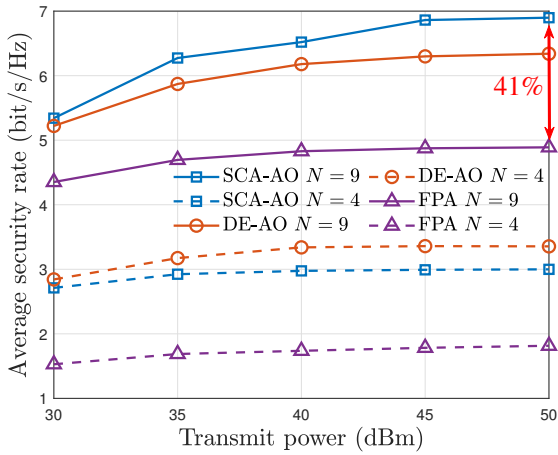


Figure 7 Average secrecy rate versus the transmit power under different antenna schemes.

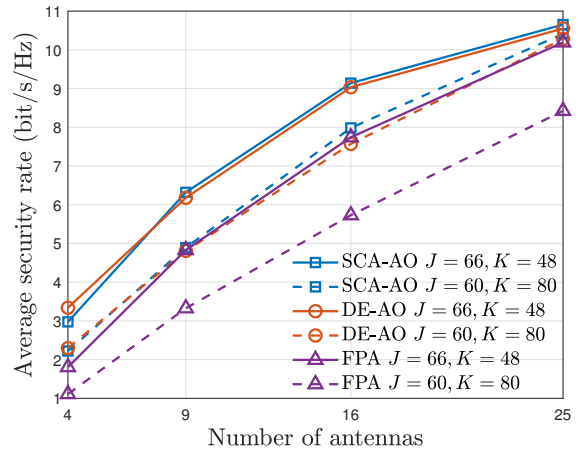


Figure 8 Average secrecy rate versus the number of antennas under different satellite configurations.

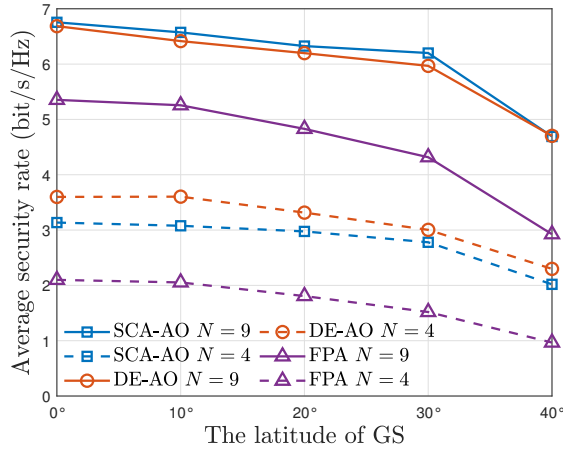


Figure 9 Average secrecy rate versus the latitude of GS under different antenna schemes.

secrecy rate, as the enlarged search space reduces the effectiveness of the DE-based AO algorithm, while the SCA-based AO algorithm is better able to exploit local refinement. In addition, the average secrecy rate of all schemes decreases with the GS latitude, mainly because the satellite-ground geometry becomes less favorable and suppressing strong eavesdropping channels becomes more difficult at higher latitudes.

6 Conclusion

In this paper, we studied an MA-assisted secure uplink transmission scheme for time-varying LEO satellite communications. An average secrecy rate maximization problem was formulated by jointly optimizing the GS transmit beamforming and the MA positions. Since the formulated problem was non-convex, an AO framework was adopted to decompose it into a beamforming optimization subproblem and an MA position optimization subproblem. The beamforming subproblem was handled via SDR, while the MA position optimization subproblem was solved by an SCA-based algorithm and a DE-based algorithm. Numerical results showed that the proposed MA-assisted LEO satellite secure transmission scheme achieved clear secrecy rate gains over the FPA scheme. It was also observed that DE performed better with a small number of antennas due to its global search capability, whereas its effectiveness decreased as the number of antennas increased because of the enlarged search space, allowing SCA to achieve superior performance.

Acknowledgements

Supporting information Appendix A. The supporting information is available online at info.scichina.com and link.springer.com. The

supporting materials are published as submitted, without typesetting or editing. The responsibility for scientific accuracy and content remains entirely with the authors.

References

- 1 Al-Hraishawi H, Chougrani H, Kisseleff S, et al. A survey on nongeostationary satellite systems: The communication perspective. *IEEE Communications Surveys & Tutorials*, 2022, 25: 101–132
- 2 Giordani M, Zorzi M. Non-terrestrial networks in the 6G era: Challenges and opportunities. *IEEE network*, 2020, 35: 244–251
- 3 Miao H, Zhang J, Tang P, et al. Sub-6 GHz to mmWave for 5G-advanced and beyond: Channel measurements, characteristics and impact on system performance. *IEEE Journal on Selected Areas in Communications*, 2023, 41: 1945–1960
- 4 Kang M, Park S, Lee Y. A survey on satellite communication system security. *Sensors*, 2024, 24: 2897
- 5 Singh R, Ahmad I, Huusko J. The role of physical layer security in satellite-based networks. In: *Proceedings of 2023 Joint European Conference on Networks and Communications & 6G Summit (EuCNC/6G Summit)*. IEEE, 2023. 36–41
- 6 Xu H, Zhang J, Tang P, et al. Near-field propagation and spatial non-stationarity channel model for 6-24 GHz (FR3) extremely large-scale MIMO: Adopted by 3GPP for 6G. *IEEE Journal on Selected Areas in Communications*, 2026
- 7 Shiu Y S, Chang S Y, Wu H C, et al. Physical layer security in wireless networks: A tutorial. *IEEE wireless Communications*, 2011, 18: 66–74
- 8 Lu W, An K, Liang T. Robust beamforming design for sum secrecy rate maximization in multibeam satellite systems. *IEEE Transactions on Aerospace and Electronic Systems*, 2019, 55: 1568–1572
- 9 Cui G, Zhu Q, Xu L, et al. Secure beamforming and jamming for multibeam satellite systems with correlated wiretap channels. *IEEE Transactions on Vehicular Technology*, 2020, 69: 12348–12353
- 10 Bankey V, Upadhyay P K. Physical layer security of multiuser multirelay hybrid satellite-terrestrial relay networks. *IEEE Transactions on Vehicular Technology*, 2019, 68: 2488–2501
- 11 Huang M, Gong F, Zhang N, et al. Reliability and security performance analysis of hybrid satellite-terrestrial multi-relay systems with artificial noise. *IEEE Access*, 2021, 9: 34708–34721
- 12 Li J, Han S, Tai X, et al. Physical layer security enhancement for satellite communication among similar channels: Relay selection and power allocation. *IEEE Systems Journal*, 2019, 14: 433–444
- 13 Na D H, Park K H, Ko Y C, et al. Physical layer security for LEO satellite communication systems with friendly jamming satellite. *IEEE Transactions on Wireless Communications*, 2025
- 14 Bueno F A D, Khoshafa M H, Ngatched T M. Physical layer security in RIS-assisted THz-enabled LEO satellite communications. *IEEE Open Journal of the Communications Society*, 2025
- 15 Jiang X, Yan P, Li B, et al. Physical layer security for practical RSMA-based hybrid satellite-terrestrial relay networks. *IEEE Transactions on Vehicular Technology*, 2025
- 16 Zhu L, Wong K K. Historical review of fluid antenna and movable antenna. *arXiv preprint arXiv:2401.02362*, 2024
- 17 Zhu L, Pi X, Ma W, et al. Dynamic beam coverage for satellite communications aided by movable-antenna array. *IEEE Transactions on Wireless Communications*, 2024, 24: 1916–1933
- 18 Zhu L, Ma W, Mei W, et al. A tutorial on movable antennas for wireless networks. *IEEE Communications Surveys & Tutorials*, 2025
- 19 Zheng J, Zhang J, Du H, et al. Flexible-position MIMO for wireless communications: Fundamentals, challenges, and future directions. *IEEE Wireless Communications*, 2024, 31: 18–26
- 20 Li Y, Xu H, Zeng M, et al. Pinching antenna-aided wireless powered communication networks. *IEEE Wireless Communications Letters*, 2026, 15: 255–259
- 21 Tang B, Xu H, Wong K K, et al. Fluid antenna enabling secret communications. *IEEE Communications Letters*, 2023, 27: 1491–1495
- 22 Xu H, Wong K K, New W K, et al. Coding-enhanced cooperative jamming for secret communication in fluid antenna systems. *IEEE Communications Letters*, 2024, 28: 1991–1995
- 23 Zhu L, Ma W, Zhang R. Modeling and performance analysis for movable antenna enabled wireless communications. *IEEE Transactions on Wireless Communications*, 2023, 23: 6234–6250
- 24 Xiao J, Wang J, Liu Y. Channel estimation for pinching-antenna systems (PASS). *IEEE Communications Letters*, 2025, 29: 1789–1793
- 25 Hu G, Wu Q, Xu K, et al. Secure wireless communication via movable-antenna array. *IEEE Signal Processing Letters*, 2024, 31: 516–520
- 26 Tang J, Pan C, Zhang Y, et al. Secure MIMO communication relying on movable antennas. *IEEE Transactions on Communications*, 2024, 73: 2159–2175
- 27 Ding J, Zhou Z, Jiao B. Movable antenna-aided secure full-duplex multi-user communications. *IEEE Transactions on Wireless Communications*, 2025, 24: 2389–2403
- 28 Hu G, Wu Q, Xu D, et al. Movable antennas-assisted secure transmission without eavesdroppers' instantaneous CSI. *IEEE Transactions on Mobile Computing*, 2024, 23: 14263–14279
- 29 Liu P, Si J, Cheng Z, et al. Movable-antenna enabled covert communication. *IEEE Wireless Communications Letters*, 2024, 14: 280–284
- 30 Lin L, Ding J, Zhou Z, et al. Power-efficient full-duplex satellite communications aided by movable antennas. *IEEE Wireless Communications Letters*, 2024, 14: 656–660
- 31 Wang J, Zhu L, Han S, et al. Joint antenna positioning and beamforming for movable antenna array aided ground station in low-earth orbit satellite communication. *IEEE Transactions on Wireless Communications*, 2025, 25: 9437–9451
- 32 Li Y, Wang J, Zou Y, et al. Weighted sum power maximization for STAR-RIS assisted SWIPT systems. *IEEE Transactions on Wireless Communications*, 2024, 23: 18394–18408
- 33 Zhang Y, You C, So H C. Movable-antenna position optimization: A new evolutionary framework. *IEEE Transactions on Wireless Communications*, 2025